Guest – Framework Interaction in Type I Inorganic Clathrates with Promising Thermoelectric Properties: On the Ionic versus Neutral Nature of the Alkaline-Earth Metal Guest A in $A_8Ga_{16}Ge_{30}$ (A = Sr, Ba)

Carlo Gatti,*[a] Luca Bertini,[a] Nick P. Blake,[b] and Bo B. Iversen[c]

Abstract: Periodic density functional calculations using pseudopotentials and a local basis set were performed on the type I clathrates $A_8Ga_{16}Ge_{30}$ (A = Sr, Ba). Both are known to show promising thermoelectric properties. Ab initio wave functions were analyzed within the framework of the quantum theory of atoms in molecules. This enabled us to analyze both the charge transfer and bonding properties of the clathrate from a rigorous quantum mechanical viewpoint. The Ba and Sr centers were found to be largely ionic (charge: ca. +1.7 e) both in the smaller 20-atom and in the larger 24-atom cages, consistent with a Zintl-phase view of these type I clathrates. The assertion that the Sr atoms in the different cages have similar oxidation states is shown to be consistent with multiwavelength diffraction experiments on $Sr_8Ga_{16}Ge_{30}$; while the assertion of ionicity of the Sr center is supported by the observation that the adsorption edge lies close to that previously found in the Sr K-edge XANES spectra of $Sr(OH)_2 \cdot 8H_2O$. As such, this work contradicts previous experimental and theoretical studies that claim that the guest atoms are neutral. We show that the discrepancy is related to the definitions used for electron transfer. Definitions based on electron displacement (rearrangement) in space, as in previous works, do not account for the variation in shape and volume of the atomic catchment regions upon change in the number and average locations of the particles in the system. Eventually, such definitions lead to underestimation of charge transfer. The large binding energy found in earlier work for Ba and Sr in these materials is found to be consistent with a simple picture of charge transfer from the guest to the frame. Preliminary investigations on a clathrate of perfect stoichiometry appear to rule out any important relationship between the observed increase in the thermoelectric figure of merit with increasing external pressure and host – guest charge transfer.

Keywords: ab-initio calculations · clathrates · host – guest systems · thermoelectric materials · Zintl phases

Introduction

In the search for promising thermoelectric materials (TMs), in the last five years, many scientists have focussed on the rare-earth-filled skutterudites and type I inorganic clathrates. These semiconducting materials seem to fulfil Slack's phonon glass and electron crystal (PGEC) criterion[1, 2] for a good TM. Type I clathrates, which are the topic of this paper, show some promise for high-temperature thermoelectric applications. They consist of two types of cages, the 20-atom dodecahedron and the 24-atom tetradodecahedron (Figure 1). The stoichiometry is generally written as $A_xB_yC_{46-y}$, where B and C are Group 3 and 4 elements, respectively, and A is an alkali or alkaline earth metal. These metal atoms are encapsulated in the cages formed by the framework of tetrahedrally bonded atoms B and C. The encapsulated atoms are known to possess localized, low-frequency phonon modes that lower the thermal conductivity k to values comparable to those of amorphous semiconductors.[3–5] It is believed, although not theoretically demonstrated, that these phonon modes do not significantly affect the electrical conductivity σ. If true, this may explain why carrier mobilities are comparable to those of crystalline semiconductors,[6] and would confirm clathrates as prototypical PGECs.

Recently, experimental and theoretical studies have appeared on $A_8Ga_{16}Ge_{30}$ (A = Sr, Ba) concerning their structure and stability,[7–10] band structure and thermoelectric properties,[8, 11] and anisotropic vibrations of the metal guest.[3, 8, 10, 12] A dramatic positive effect[13] on the figure of merit when an external pressure of 7.5 GPa was applied to n-doped $Sr_8Ga_{16}Ge_{30}$ has also been reported.

[a] Dr. C. Gatti, Dr. L. Bertini
CNR-ISTM, Istituto di Scienze e Tecnologie Molecolari
via C. Golgi 19, 20133 Milano (Italy)
Fax: (+39) 2-50314300
E-mail: c.gatti@istm.cnr.it

[b] Dr. N. P. Blake
Department of Chemistry and Biochemistry, University of California
Santa Barbara, CA 93106 (USA)

[c] Dr. B. B. Iversen
Department of Chemistry, University of Aarhus
8000 Aarhus C (Denmark)

DOI: 10.1002/chem.200304837

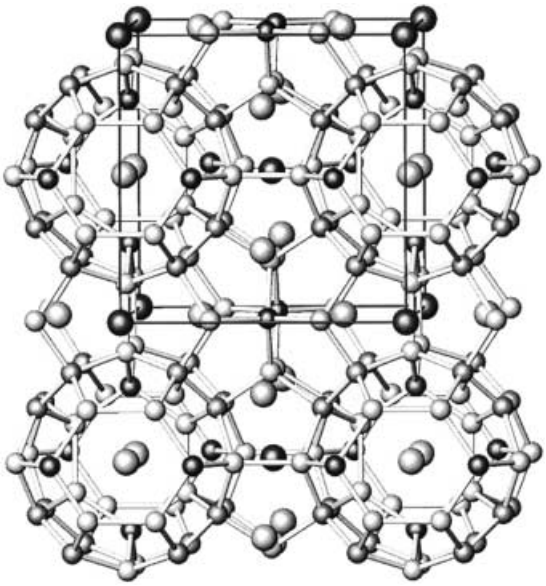

Figure 1. The clathrate type I structure.

Structural chemists generally regard these clathrates as Zintl phases,[14] in which the guest atoms completely transfer/accept valence electrons to/from the framework. The observation that the clathrate type I structures exhibit a fixed number of valence electrons per unit cell (184 e), despite the large variation in their elemental compositions, firmly supports this belief.

Indeed, band structure calculations[9] of the Ba_8 and $Ga_{16}Ge_{30}$ sublattices showed that the metal functions as an electron donor; this accounts for the semiconducting Zintl nature of $A_8Ga_{16}Ge_{30}$. Transport calculations[11] for the Zintl phase stoichiometries indicated (albeit within the relaxation-time approximation) that clathrates showed promise as high-temperature thermoelectrics. However, when the charge density of the clathrate was compared with that for interleaved, noninteracting Ba_8 and $Ga_{16}Ge_{30}$ sublattices, it was surprisingly found[9] that while Ba was clearly an electron donor it did not appear to be ionic. Charges on a given Ba atom in the clathrate and Ba_8 were calculated by evaluating the total electron charge within a sphere of a given radius around a given Ba nucleus and were found to be rather similar. Analysis of the experimental electron density of the Sr clathrate with a maximum-entropy method (MEM) also supported the idea of nonionic metal guests in these clathrates.[10] This belief was not contradicted by XANES data at the Sr K-edge, which revealed an edge position for the clathrate similar to that of Sr metal, although the absorption edge was very broad.[10]

This paper re-examines this "ionic versus neutral debate" within the framework of the quantum theory of atoms in molecules (QTAIM).[15] This approach, being fully rooted in quantum mechanics,[15, 16] has the advantage that it is free from any arbitrariness in defining and determining the volume, shape and resulting electron population of any atomic basin in a compound. The QTAIM approach was also used to characterize the nature of the bonding of the metal guests to the frame. We shall demonstrate that both Ba and Sr are best thought of as ionic, thus reconciling the Zintl view of the title clathrates with what is expected from the notions of elementary chemistry. In the case of $Sr_8Ga_{16}Ge_{30}$ we compare our estimate of the charge transfer with the results of a multiwavelength diffraction experiment across the Sr K-edge to see if the experimental observations can be rationalized from this new viewpoint. Finally, we investigate the pressure dependence of this charge transfer between the metal and the frame to see if this in part is responsible for the dramatic enhancement in the figure of merit observed when an external pressure is applied to *n*-doped $Sr_8Ga_{16}Ge_{30}$.[13]

Computational and Experimental Methods

Geometries of investigated systems: *$A_8Ga_{16}Ge_{30}$ ($A = Sr$, Ba)*: Two structures for each clathrate, corresponding to two different Ga atom sitings in the framework and with zero and four Ga–Ga bonds were considered (see Table 1). The geometries of these structures were taken from a previous study[9] in which a full minimization of atomic positions and cell volumes was performed by using a density functional generalized-gradient approach (GGA) and a plane-wave basis set. The space group of the considered structures is *P*1 (no. 1), while the framework sites reported in Table 1 are labeled according to the $Pm\bar{3}n$ symmetry of the idealized and fully symmetric $A_8Ga_{16}Ge_{30}$ clathrate in which no distinction is made between Group 3 and Group 4 elements. Such a clathrate, hereinafter referred to as the parent clathrate PC, has only three types of framework sites (6*c*, 16*i*, and 24*k*) and two different locations (2*a* and 6*d*) for the guest cations at the center of the 20-atom and 24-atom cages, respectively.

Table 1. Labeling and relative energy of the P1 $A_8Ga_{16}Ge_{30}$ clathrates for different Ga sittings at the *c*, *i* and *k* special positions of the $Pm\bar{3}n$ space group.

Label	#6*c*	#16*i*	#24*k*	#Ga–Ga[a]	ΔE [eV][9]		ΔE [eV], this work	
					A = Sr	A = Ba	A = Sr	A = Ba
B1	3	1	12	0	0.00	0.00	0.00	0.00
B3	5	3	8	4	0.52	0.42	3.99	1.90
parent	0	16	0	8	–	–	10.00	–

[a] Number of Ga–Ga (short) bonds.

Preliminary tests to select the optimum basis set and other computational conditions were performed on the $Sr_8Ga_{16}Ge_{30}$ PC, since this model system allows for a drastic reduction of computational time, due to the 48 symmetry operations of the $Pm\bar{3}n$ space group. Model cell parameter and free fractional coordinates (*i* and *k* positions) of the PC were taken from a 20 K synchrotron X-ray diffraction experiment.[17]

A_8 ($A = Sr$,Ba); bulk Ga and Ge: These systems were calculated either for determining the optimum basis set and computational conditions (vide infra) or as a source of reference bonding and atomic properties to be compared with those observed in the investigated clathrates. A_8 was assigned the symmetry, cell parameters and atom coordinates of the B1 clathrate (see Table 1), while the geometries of Ga (space group *Cmca*, no. 64) and Ge (space group *Fd3m*, no. 227) were taken from reference [18].

AO ($A = Sr$,Ba): These oxides were investigated in their B_1 NaCl-type phases (space group *Fm3m*, no. 225) and at their experimental geometries[19] as prototypical cases in which the A metal atoms are almost fully ionized.

Hamiltonians and *k*-point sampling: Calculations were performed using the Hartree–Fock–Roothaan or the density functional Kohn–Sham approach, as implemented in the CRYSTAL98 code.[20] Several density functional correlation and exchange potentials were adopted in the preliminary tests on the parent clathrate. The Perdew–Wang[21] and

Becke[22] GGA functionals (hereinafter collectively termed PWB) were then used as correlation and exchange potentials, respectively, for calculations on the P1 geometry clathrates. The Fock or Kohn–Sham matrix was diagonalized at an isotropic net of $6 \times 6 \times 6$ k-points, while $12 \times 12 \times 12$ k-points were used in the reciprocal space integration for Fermi energy calculation and density matrix reconstruction.

Effective core pseudopotentials: Preliminary tests on the parent and on the P1 clathrates used the large-core pseudopotentials (LCPP) of Wadt and Hay[23] for all types of atoms. However, difficulties in the analysis of the resulting electron density (ED) topologies (see ref. [24] for a discussion of the effect of pseudopotentials on the ED distributions), led us to adopt a Hay–Wadt[25] small-core pseudopotential (SCPP) for the A atoms, while retaining the LCPP for the framework atoms, in the final calculations. The LCPP is the only pseudopotential available for Ge and Ga within the Hay–Wadt scheme.

All-electron computations: $Sr_8Ga_{16}Ge_{30}$ in the B1 geometry was also calculated by including all electrons of the Ga and Ge atoms in the self-consistent procedure, while retaining the SCPP for the Sr atoms. A standard STO-3G basis set[26] was used for Ga and Ge, while basis set D (vide infra) was used for the Sr atom. This computation is referred to as AEPP in the following.

Independent atom model (IAM) computations: For the sake of comparison of the self-consistent ab initio results with a case in which no spatial charge transfer with respect to the isolated atoms is allowed, we calculated the electron density in the crystal using a periodic density matrix obtained as a superposition of atomic densities (PATO option in CRYSTAL98) and the same basis set as in the crystal calculation. To each atomic solution, the neutral-atom population was assigned.

Basis sets: In the preliminary LCPP computations, the original 3s3p/1s1p Wadt–Hay[23] energy-optimized valence basis sets were adopted. These basis sets led to long CPU times even for the high-symmetry parent clathrate, thus making the computation of the P1 clathrates nearly prohibitive. To decrease CPU times, the following procedure was followed.

1) The s = p constraint was imposed on the atomic shells of all atoms, and the Gaussian exponents used were those of the s basis functions in the original Hay–Wadt basis sets.[23, 25] The new M contraction coefficients ($M = 3$ for Ga, Ge; $M = 5$ for Sr, Ba) for each of the ns ($n = 4$ for Sr, Ga, Ge; $n = 5$ for Sr, Ba, $n = 6$ Ba) and np functions ($n = 4$ for Sr, Ga, Ge; $n = 5$ for Ba) were determined by HFPP atomic calculations with the Hay–Wadt LC (Ga,Ge) or SC (Sr, Ba) pseudopotentials. This step yielded basis set B, where basis set A denotes the original SC (Sr,Ba) and LC (Ga,Ge) Hay–Wadt basis sets.
2) The outermost s Gaussians (Sr: $\alpha = 0.0292$; Ba: $\alpha = 0.0231$) of the ns expansions of Sr and Ba S-PP original basis sets were removed. Using the s = p constraint for the remaining four s primitives, the new ns and np contraction coefficients for Sr and Ba were obtained with the procedure given earlier. This step led to basis set C (Ga and Ge basis sets are the same as in basis set B).
3) The optimum scale factors (SFs) for the outermost sp shell of Ga and Ge to be used in the clathrate calculations were variationally determined from DFT-PWB computations on Ga and Ge metals. Using the thus-obtained SF for Ge (1.02) and Ga (0.98) the SF for the outermost 5s shell of Sr (1.02) was variationally determined from DFT-PWB computations on the parent clathrate. An SF of 1.0 was used for the outermost 6s shell of Ba. This step led to basis set D.

Table 2 shows how the computing time for the parent clathrate decreases from basis set A to basis set C. Table 2 also shows that with basis set D the CPU time for calculating the P1 clathrate at B1 geometry has become acceptable and comparable to that required for the parent clathrate with basis set A.

Table 2. $Sr_8Ga_{16}Ge_{30}$, DFT-BECKE-PWGGA: total energy and CPU time as a function of space group symmetry and basis set.

Space group	Basis set	Energy [a.u.]	CPU time [s]
$Pm\bar{3}n$, Parent clathrate	A	– 391.41368	57952
	B	– 390.80914	8408
	C	– 390.80380	1507
P1, geometry B1	D	– 391.09053	140338

For the SrO and BaO reference systems, several basis sets and approaches were considered.

1) Test 1 (T1): The oxygen atom was described with an all-electron basis set, while for Sr and Ba the SC Hay–Wadt pseudopotential was adopted. Basis sets were taken from a detailed study[27] on the phase transition from B_1 (NaCl type) to B_2 (CsCl type) phases in alkaline-earth oxides. The oxygen basis was an 8-411-(1d)G contraction (the first shell is of s type and is a contraction of eight Gaussian-type functions (GTFs), and there are three sp shells and one d shell), while the Sr or Ba basis is a 3-1(1d)G contraction. The optimized exponents of the two most diffuse sp and d shells of each atom and for each kind of oxide were taken from Table 1 of ref. [27].
2) Test 2 (T2): Same as T1, except for the use of basis set C (see earlier) for Ba and Sr.
3) Test 3 (T3): The standard 3-21G basis set[28] for O and Sr was modified to 3-11 for the Sr atom by splitting the two GTFs of the innermost valence sp shell and by removing the outermost valence GTF. The exponent of the outermost GTFs for Sr and O atoms were then iteratively optimized using a numerical steepest descent gradient optimisation as implemented in the LoptCG code,[29] interfaced to CRYSTAL98. Final optimized exponents were 0.335 and 0.092 for O and Sr, respectively. A restricted Hartree–Fock (RHF) approach was used.
4) Test 4 (T4): Same as T3, except for the use of the DFT-PWB Hamiltonian instead of the RHF type. Due to the insufficient numerical accuracy achieved in the LoptCG optimisation of the outermost GTF of Sr using the DFT approach, the basis set optimized in test T3 was adopted.

Electron density analysis: Atomic net populations and guest–frame bond properties were determined by a topological analysis of the electron density, according to the QTAIM theory.[16] Application of QTAIM to our crystalline wave functions was made possible by the code TOPOND98,[30] interfaced to CRYSTAL98. The accuracy of the numerical determination of integrated properties was judged against the calculated values for the atomic Lagrangian $L(\Omega) = -(1/4)\int_\Omega \nabla^2\rho$, a quantity that should vanish because of the atomic-basin boundary condition.[15] The obtained values of $L(\omega)$ were typically less than 1×10^{-4} a.u. Atomic net populations for the IAM density were also evaluated through TOPOND98, by supplying to this code the density matrix obtained with the PATO option of CRYSTAL98.

Multiwavelength diffraction experiment: The variation in the anomalous part of the atomic scattering factor $f(S)$ ($f(S) = f^0(S) + f' + if''$) across an absorption edge can be used to create contrast between atoms of the same element in different valence states.[31] This is because the ionization energies and thus the position of the absorption edge depends on the oxidation state of the system. The energy dependence of the Bragg reflection intensity near and above the absorption edge of some atomic level forms the basis of the diffraction anomalous fine-structure (DAFS) method.[32] This technique combines the sensitivity to long-range order typical of the X-ray diffraction method with the local character and site selectivity of absorption spectroscopy. The DAFS technique, if applied to a selection of reflections in an energy range near and above the absorption edge, should represent a valuable experimental tool for shedding light, in a site-specific manner, on the guest valence states in clathrates. In the present case we used a somewhat different approach than in the typical DAFS experiment. Instead of collecting a few reflections at many different wavelengths and relying on somewhat crude absorption correction and the Kramers–Kronig transformation to obtain f', we collected many reflections at relatively few wavelengths around the Sr K-edge. This allows us to obtain f' directly as a parameter in the crystallographic refinements.

The multiwavelength diffraction experiment was carried out on $Sr_8Ga_{16}Ge_{30}$ at the Swiss-Norwegian beam line at the European Synchrotron Radiation Facility, on a crystal with maximum dimensions of about 25 μm to minimize absorption and extinction effects. Full structural diffraction data were collected at 10 wavelengths across the Sr K-edge as well as at one very short wavelength (off-edge).[33] Details of the experimental data are listed in Table 3. The data were carefully selected to contain: i) all the low-order reflections ($\sin\theta/\lambda < 0.3$ Å^{-1}), ii) – enough symmetry-equivalent reflections to carry out accurate empirical absorption corrections[34] and iii) a selection of high-order reflections predicted to have large changes in the anomalous scattering contribution f' across the Sr K-edge.[35] The data set collected at short wavelength ($\lambda = 0.49994$ Å) was used to establish the positional and thermal parameters of the structure

Table 3. Details of the multiwavelength crystallographic experiment on $Sr_8Ga_{16}Ge_{30}$. The refinements were carried out in space group $Pm\bar{3}n$ (a = 10.72933(9) Å) with Sr(d) disordered over four sites (24j). In all refinements the guest atom occupancies were fixed at 100%. The X-ray path lengths are based on refined crystal dimensions during the absorption correction procedure.[61] They are in excellent agreement with the crystal size and shape observed under a light microscope prior to mounting and under an electron microscope after mounting. The internal agreement factor is defined as in the equation $R_I = \Sigma | I - \langle I \rangle | / \Sigma | I |$.

$E_{X\text{-ray}}$ [eV]	λ [Å]	μ_l [mm^{-1}]	Max./min. XPL[a] [μm]	Max./min. XTF[b]	R_I	N_{meas}	N_{uniq}	N_{var}	$f'_{Sr\ atom}$ (calcd)	$f'_{Sr(a)}$ (exptl)	$f'_{Sr(d)}$	R_F	R_{F^2}	R_{wF^2}	GoF
16099	0.77014	33.6	7/28	0.40/0.80	0.0257	330	101	4	−7.5	−7.74(7)	−7.5(7)	0.045	0.056	0.146	1.52
16103	0.76995	33.5	5/27	0.40/0.84	0.0272	374	104	4	−8.8	−8.4(4)	−8.0(3)	0.035	0.047	0.084	0.86
16105	0.76986	42.7	6/24	0.36/0.79	0.0290	340	104	4	−10.3	−9.2(8)	−8.9(7)	0.053	0.078	0.151	1.45
16107	0.76976	42.7	7/28	0.31/0.74	0.0368	775	150	4	−8.39	−10.2(7)	−9.8(6)	0.078	0.106	0.157	1.33
16109	0.76966	42.7	9/27	0.31/0.67	0.0284	589	150	4	−7.76	−10.1(3)	−9.4(3)	0.041	0.067	0.079	0.73
16111	0.76957	42.7	8/28	0.31/0.71	0.0243	439	112	4	−7.37	−9.3(4)	−9.0(4)	0.047	0.071	0.095	0.97
16113	0.76947	42.7	5/26	0.33/0.81	0.0229	320	102	4	−7.09	−10.3(10)	−9.2(19)	0.057	0.060	0.205	1.92
16115	0.76938	42.7	6/26	0.34/0.79	0.0268	388	112	4	−6.86	−8.1(5)	−8.7(5)	0.055	0.077	0.106	1.01
16118	0.76923	42.7	7/28	0.31/0.74	0.0317	580	103	4	−6.60	−7.4(3)	−7.1(3)	0.034	0.044	0.072	0.72
16123	0.76900	42.6	2/25	0.35/0.92	0.0340	351	103	4	−6.27	−7.1(6)	−6.4(5)	0.047	0.059	0.124	1.14
24800	0.49994	13.2	9/32	0.66/0.89	0.0268	1094	143	19	−0.023			0.045	0.022	0.044	0.53

[a] X-ray path length. [b] X-ray transmission factor.

with little influence of systematic errors.[36] In the refinement of the 10 Sr K-edge data sets, the structural parameters and the extinction parameter were fixed at the values obtained from the off-edge data, and only the scale factor and the anomalous scattering contributions for the two separate Sr sites were refined.[37]

Results

Data in Table 1 confirm[9] that the clathrate structure B1, with no short Ga–Ga contacts, is the most stable among the investigated structures for both Sr and Ba guests. The energy difference between structures B1 and B3 is somewhat larger than found previously,[9] likely due to the use of geometries which were not fully optimized for the computational model adopted in this study.

Guest-to-frame charge transfer: Table 4 lists a number of atomic properties, averaged over the basins of the guest atoms in the 20- or in the 24-atom cage, for the B1 and the B3 structures of $A_8Ga_{16}Ge_{30}$. Atomic properties were calculated from the DFT-PWB wave function with basis set D. For the sake of comparison, Table 4 also reports the corresponding atomic properties, at the B1 geometry, for the A_8 sublattices and for $A_8Ga_{16}Ge_{30}$ clathrates, obtained with the AEPP approach or the IAM model. Table 5 displays results for charge transfer in SrO and BaO for tests T1–T4.

Table 4. Averages (standard deviations) of atomic basin properties of alkaline earth metal atoms A (A = Sr, Ba) in the $A_8Ga_{16}Ge_{30}$ clathrates at geometries B1 and B3 for ab initio and IAM models. For the sake of comparison data for the A_8 sublattices are also reported. All quantities in a.u.

Model//basis set	Ω	Pos.[a]	$q(\Omega)$[b]	BV2[c]	TBV[c]	SPHD[d]	ρ_{av}[e]	r_{sph}[f]
$A_8Ga_{16}Ge_{30}$, geometry B1								
DFT-BECKE-PWGGA//D	Sr	*a*	+1.669 (0.001)	135.3 (0.0)	135.3 (0.0)	0.86 (0.00)	0.269	3.18 (0.00)
		d	+1.687 (0.005)	154.9 (2.6)	157.5 (1.0)	0.88 (0.01)	0.231	3.35 (0.01)
	Ba	*a*	+1.743 (0.001)	161.2 (0.2)	161.2 (0.2)	0.81 (0.00)	0.337	3.38 (0.00)
		d	+1.773 (0.003)	194.2 (0.8)	194.3 (0.7)	0.85 (0.00)	0.279	3.59 (0.00)
AEPP(basis set, see text)	Sr	*a*	+1.769	146.1	146.1	0.89	0.248	3.27
		d	+1.744	156.7	178.3	0.91	0.203	3.49
IAM//D	Sr	*a*	−0.096	201.3	201.3		0.189	3.64
		d	−0.126	241.6	241.6		0.158	3.86
	Ba	*a*	+0.858	186.3	186.3		0.296	3.54
		d	+0.576	251.8	251.8		0.220	3.92
$A_8Ga_{16}Ge_{30}$, geometry B3								
DFT-BECKE-PWGGA//D	Sr	*a*	+1.658 (0.001)	134.1 (0.0)	134.1 (0.0)	0.86 (0.00)	0.271	3.18 (0.01)
		d	+1.677 (0.009)	152.3 (2.2)	157.4 (1.0)	0.88 (0.00)	0.231	3.35 (0.01)
	Ba	*a*	+1.740 (0.003)	160.8 (0.0)	160.8 (0.0)	0.81 (0.00)	0.337	3.37 (0.00)
		d	+1.769 (0.007)	194.2 (0.6)	194.3 (0.6)	0.85 (0.00)	0.279	3.59 (0.00)
A_8, geometry B1								
DFT-BECKE-PWGGA//D	Sr	*a*	0.000	324.9	1066.1	1.00	0.036	6.34
		d	0.000	326.4	1095.4	0.99	0.035	6.39
	Ba	*a*	0.000	444.1	1095.7	0.97	0.051	6.40
		d	0.000	445.2	1131.4	0.97	0.049	6.46

[a] The special position that the A atom would occupy in space group 223 ($Pm\bar{3}n$), with a and d corresponding to the centers of the 20- and 24-atom cages, respectively. [b] $q(\Omega)$ is the net charge in basin Ω. [c] TBV is the total basin volume, while BV2 is the volume of that portion of the basin in which the electron density is equal to or exceeds 0.002 a.u. [d] SPHD, given by $\mathrm{SPHD} = \int_\Omega \boldsymbol{r}\cdot\nabla\rho / [-3N(\Omega)]$, where $N(\Omega)$ is the basin electron population, attains the limit of 1 in an isolated atom and in the limit of an extremely loosely bound atom (see ref. [40]). [e] ρ_{av} is the average electron density in Ω, given by $[N(\Omega) + N_c(\Omega)]$/BTV where $N_c(\Omega)$ is the number of frozen electrons in the pseudopotential calculation. [f] r_{sph} is the radius of a sphere with a volume equal to the BTV.

Table 5. Atomic basin properties of alkaline earth metal atoms A (A = Sr, Ba) in their oxides AO for tests T1 – T4. All quantities in a.u., symbols and abbreviations as in Table 4.

Test	Ω	$q(\Omega)$	BV2	BTV	SPHD	ρ_{av}	r_{sph}
T1	Sr	+1.543	113.3	113.3	0.84	0.321	3.00
T2		+1.717	110.7	110.7	0.83	0.328	2.98
T3		+1.871	110.5	110.5	0.97[a]	0.327	2.98
T4		+1.782	110.6	110.6	0.96[a]	0.327	2.98
T1	Ba	+1.510	164.6	164.7	0.80	0.331	3.40
T2		+1.758	155.3	155.3	0.80	0.349	3.33

[a] Due to the inclusion of the core-electron contribution, which has nearly perfect spherical symmetry, SPHD has a much higher value in tests T3 and T4, compared to those obtained in tests T1, T2 and for A atoms in the clathrates.

Atomic net charges $q(\Omega)$ in Tables 4 and 5 were obtained from $q(\Omega) = Z_{eff}(\Omega) - N(\Omega)$, where Z_{eff} is the effective nuclear charge[38] of the atom and $N(\Omega)$ is its electron population, given by the integral of the electron density over the atomic basin Ω. The atomic basin is the portion of space including the atomic nucleus and enclosed by a surface S defined by the zero-flux condition[15] as in the equation $\nabla\rho(\boldsymbol{r}_s)\cdot\boldsymbol{n}(\boldsymbol{r}_s) = 0$ where $\boldsymbol{n}(\boldsymbol{r}_s)$ is a unit vector normal to the surface at $\boldsymbol{r}_s$, and $\boldsymbol{r}_s$ denotes any point of the surface S. The thus-defined atomic basins are proper quantum objects, and their electron populations are quantum observables,[16] provided the electron density ρ used in the basin definition is obtained from an ab initio wave function. This property ensures that the net charges in Tables 4 and 5, except for those derived from the IAM model, have a well-defined physical meaning. The main results we obtained are summarized below.

1) The guest atoms in the $A_8Ga_{16}Ge_{30}$ clathrates are almost completely ionized, regardless of the kind of cage they occupy.[39] Their net charge is about +1.7 e, and the charge difference between the two cages is indeed very small (ca. 0.02 e) and similar for Ba and Sr clathrates.
2) As expected, Ba atoms are slightly more ionized than Sr atoms since they loose an additional 0.1 e in both cages with respect to Sr.
3) The results listed above hold true whether the Ga and Ge core electrons are included (DFT-PWB) or not included (AEPP) in the self-consistent field (SCF) procedure.
4) The influence of the kind of Ga sitings on guest-to-frame charge transfer is rather limited, as can be appreciated by comparing results for the B1 and B3 geometries. Full geometry optimisation of B1 and B3 structures should not affect this conclusion. It should bring the charge transfer to even closer similarity, since we found an energy difference for the two structures (Table 1) which is larger than that obtained[9] with full geometry optimisation.
5) The largest difference between the two types of cages is the 13 – 18 % increase in the total basin volume (TBV) on passing from the smaller to the larger cage (Table 4). Owing to the similar net charges of the guest atoms in the two cages, this basin expansion yields a corresponding decrease in the average electron density ρ_{av} in the basin of the A atoms in the 24-atom cage. The observed increase in size of the A basins in this cage does not imply the presence of regions of very low atomic density, since TBV in this case is also very close to BV2, the volume of the portion of the atomic basin in which ρ is greater than or equal to 0.002 a.u.
6) Net charges of the guest atoms in the clathrates closely correspond to those exhibited by the corresponding atoms in the oxides. Differences in the case of the closest level of theory and basis set quality (test T2) are about 0.04 e for Sr and even less for Ba.
7) The very small standard deviations (Table 4) found for the net charges and the other atomic properties of the guest atoms located in either of the two kinds of cages suggest that the geometry perturbation related to symmetry lowering, from $Pm\bar{3}n$ to $P1$, affects the cages of either type similarly (24-atom cages are slightly more differentiated among each other).
8) The zero-flux recipe applied to the IAM model density predicts the Sr atoms to be close to neutral and Ba atoms to be less than half-charged compared to DFT-PWB and AEPP models (Table 4). While it is not required by physics (see earlier discussion) that the zero-flux recipe should necessarily predict the A atoms to be neutral for IAM densities, it is gratifying that this recipe recovers very small or small net charges when the SCF procedure and thus the electron transfer among atomic orbitals is switched off. In other words, considering the A atoms to be almost neutral in the clathrates would correspond to ignoring the charge rearrangements due to bonding in these compounds and to assign net charges only on the basis of the changes due to the superposition of frozen atomic clouds.
9) The A atoms in either of the cages have their gradient vector field $\nabla\rho$ appreciably distorted from those of isolated atoms, as indicated by the departure of SPHD ($SPHD = \int_\Omega(\boldsymbol{r}\cdot\nabla\rho)d\tau/[-3N(\Omega)]$) from the value of unity which would be attained at the limit of no interaction with the surroundings.[15, 40] This indicates that the A atom in $A_8Ga_{16}Ge_{30}$ does not simply act as a templating agent that forces the frame atoms to bind around it to form cages. Instead, the guest – framework interaction has two main effects, namely, a nonnegligible distortion of the electron density distribution of the guest atom compared to an unbound atom, and substantial CT from the guest atoms to the framework. It is noteworthy that the A atoms in the corresponding oxides (Table 5) exhibit similar, yet somewhat enhanced, distortions, while a distribution very close to that of free atoms is found (Table 4) for the A atoms in the A_8 sublattices, in agreement with their much larger atomic volumes (TBVs).

Multiwavelength diffraction: In Figure 2 the refined f' values for each of the Sr sites are plotted against wavelength. A typical DAFS spectrum shows some characteristic and well-defined structures: the cusp at the absorption edge and the extended fine-structure oscillations above it. These modulations are very similar to those observed in X-ray absorption spectroscopy (XAS), and they are interpreted on the basis of the effects induced by the local environment around the absorbing atom on the final density of states available for the photoelectron.

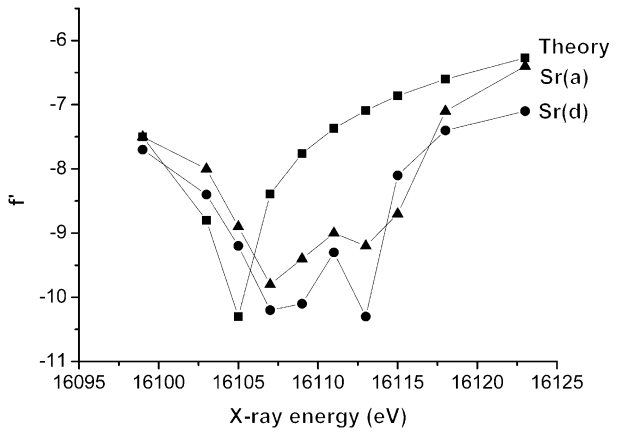

Figure 2. Plot of the refined anomalous scattering contributions f' for the two Sr sites as a function of wavelength across the Sr K-edge. The theoretical curve was calculated for a neutral Sr atom.

The curves for the two different Sr sites follow each other quite closely (Figure 2). The theoretical curve was calculated for a neutral Sr atom by using a free-atom model.[41] While this model is able to reproduce the most evident structure of f', such as the cusp, it cannot calculate the fine-structure oscillations observed in the experimental data. A model that takes these oscillations into account was recently developed in terms of the tensor formulation of the multiple scattering theory,[42] but its use is beyond the scope of the present work. The present analysis (Figure 2) indicates that the multiwavelength experiment supports similar oxidation states for the Sr atoms in the different cages, as found from ab initio wave functions. The cusp of the free-atom model occurs at somewhat lower energies than those of the Sr atoms in the two sites of the clathrate, which conversely show an adsorption edge close to that (16107 eV) obtained from the Sr K-edge XANES spectra of $Sr(OH)_2 \cdot 8H_2O$.[10]

The nature of the frame–guest interactions: Table 6 shows that in the parent clathrate (PC) the A atom hosted in the small cage is linked to 8 Ga atoms in position *i* and to 12 Ge atoms in position *k* to give a total of 20 guest–frame interactions for each A atom.[43] In the larger cages, the A atoms are only bonded to the 8 Ge atoms in position *k*. The nature of these interactions is of the closed-shell type, as indicated by the low electron density at the bond critical point (BCP) and by the dominance at the BCP of the density curvature λ_3 along the bond path over the perpendicular curvatures (λ_i, $i = 1, 2$). These features are consistent with an ionic character of these bonds.

Table 6. Guest–frame bonding interactions in the parent $A_8Ga_{16}Ge_{30}$ clathrates.[a] All quantities in a.u. if not otherwise indicated. *N* is the multiplicity of each interaction.

Bond A–B	*N*	R_{AB} [Å]	R_A [Å]	R_B, Å]	$10^2\rho_b$	$10^2\lambda_\parallel$	$\lambda_\parallel/\lvert\lambda_{\perp av}\rvert$	ε
Sr(2*a*)-Ga(*i*)	8	3.48	1.65	1.83	0.99	2.7	14.3	0.0
Sr(2*a*)–Ge(*k*)	12	3.61	1.65	1.97	0.95	2.7	14.4	3.6
Sr(6*d*)–Ge(*k*)	8	3.66	1.69	2.00	0.82	2.3	11.9	4.2
Ba(2*a*)–Ga(*i*)	8	3.51	1.75	1.76	1.12	3.0	13.7	0.0
Ba(2*a*)–Ge(*k*)	12	3.63	1.75	1.89	1.08	3.0	13.7	2.8
Ba(6*d*)–Ge(*k*)	8	3.69	1.78	1.93	0.93	2.6	11.9	2.3

[a] Cell parameter as for B1 geometry.

The bonds between guest metal atoms in either of the cages to Ge atoms in *k* positions exhibit a nonnegligible ellipticity[15] $\varepsilon = (\lambda_1/\lambda_2) - 1$, which is another indication of the departure of the electron distributions of the guest metal atoms guests from spherical symmetry. Bonds in the smaller cages are stronger and more directional than those in the larger cages, since they show a greater electron density ρ_b at the BCP and a much flatter electron density distribution in the region between two neighbouring bonds in the cage. In fact, on passing from the BCP to a point located between two neighbouring bonds and at the same distance from the guest atom A as the BCP, the electron density decreases by about 18% and by less than 1% for bonds in the 20- and 24-atom cages, respectively.

Upon release of symmetry and adoption of the minimum energy Ga atom sitings (B1 geometry), the bonding picture becomes significantly modified with respect to the PC. Table 7 reports the bond properties for the guest–frame bonding interactions averaged over the two different 20-atom and over the six different 24-atom cages associated with the B1 geometry of the clathrates. Bond properties and their standard deviations, also listed in Table 7, yield a clear and quantitative estimate of the departure from $Pm\bar{3}n$ symmetry within the two kinds of cages. The symmetry breaking is particularly relevant in the case of the 24-atom cages, and especially so for the Sr clathrate. In the large cages only 2.8(8) and 4.0(11) guest–frame bonding interactions are found on average for the Sr and Ba clathrates, respectively, instead of the eight present in the corresponding PCs. However, these remaining interactions are notably stronger than those in the PCs, as evidenced by the 50% (Sr) and 16% (Ba) average increases in the ρ_b values compared to the PCs. It is clear that the increase in strength of some interactions occurs at the expense of weakening other interactions, which ultimately disappear. We find 2–5 guest–frame bonding interactions in each large cage, and the average interaction strength within a cage decreases as the number of bonding contacts in this cage approaches that in the PCs. Also notable is the decrease in the closed-shell character of the frame-to-guest interactions with respect to those in the PCs. Indeed, the ratio of parallel to perpendicular curvatures $[\lambda_\parallel/\lvert\lambda_{\perp av}\rvert]$ is on average more than halved, as a consequence of the decreased dominance of the parallel over the perpendicular curvatures of the density at BCPs in the clathrates with B1 geometry.

The numerical decrease and the observed strengthening of the guest–frame interactions in the larger cages is not unexpected, since the A atoms are on average significantly displaced (0.81 and 0.42 Å for Sr and Ba, respectively)[9] from the center of the 24-atom cages in the B1 geometries of the clathrates. It is therefore likely that the observed symmetry lowering and displacement of the guest atoms is driven by the energy gain due to the formation of guest–frame interactions. The guest–frame interactions in the larger cages are of similar (Ba) or much greater (Sr) strength than those of the smaller cages.

It is noteworthy that the quite different guest–frame bonding features in the two kind of cages are not mirrored in significant differences in the average net charges on the

Table 7. Average[a] bond property values for the guest–frame bonding interactions in the $A_8Ga_{16}Ge_{30}$ clathrates in the B1 geometry (see text). If not otherwise stated, all quantities in a.u.

Cage	Model[b]	N_{av}	R_{av} [Å]	$(R_A)_{av}$, [Å]	$(10^2\rho_b)_{av}$	$(10^2\lambda_{\parallel})_{av}$	$(\lambda_{\parallel}/\lvert\lambda_{\perp av}\rvert)_{av}$	ε_{av}
20-atom	DFT	8(0)	3.46(2)	1.62(1)	1.03(5)	3.3(2)	3.8(8)	0.2(1)
	IAM	17(0)	3.55(8)	1.82(6)	1.55(13)	2.2(3)	3.1(15)	0.8(10)
24-atom	DFT	2.8(8)	3.38(7)	1.58(2)	1.24(13)	3.8(5)	5.8(16)	1.1(12)
		4.5(24)	1.0(20)					
				A = Ba				
20-atom	DFT	13(0)	3.54(6)	1.73(2)	1.15(8)	3.5(4)	4.0(16)	0.7(8)
24-atom	DFT	4.0(11)	3.59(13)	1.75(4)	1.08(16)	3.1(6)	3.4(17)	2.0(26)

[a] Standard deviations in parentheses. [b] DFT refers to DFT-BECKE-PWGGA//D calculations.

guest atoms within the two cages (Table 4). Net charges are the result of integration and compensating effects may thus lead to similar electron populations.

The charge rearrangement due to the guest–frame interactions may be also highlighted (Table 7) by comparing the BCP properties of the clathrates with those one would obtain (IAM model) at the limit of null interaction among the atoms forming the clathrate, except for that due to the overlap of their undistorted atomic densities. Since the A atoms are mostly ionized in the clathrate and their atomic volumes are consequently smaller than those obtained from the IAM model densities (Table 4), we expect that the A–Ge(Ga) BCPs will come closer to the A nuclei when the atomic interactions are switched on.[44] Indeed (Table 7), in the IAM density the Sr–Ge(Ga) BCPs are somewhat closer to Ge(Ga) than to the Sr atoms, whilst the opposite is true for the ab initio density. These BCP displacements of about 0.2 Å in both kinds of cage contribute to changing the Sr atoms from almost neutral to doubly ionized. In the Ba clathrate the BCP displacements are smaller (ca. 0.04 Å), consistent with the smaller change in the atomic charge of Ba on going from IAM to ab initio densities. The larger values found by the IAM model for the density at the BCPs are not an indication of stronger host–guest interactions, which are by definition absent in the IAM model, but just reflect the increase in electron density when the BCP locations come closer to the framework atoms.

Discussion

Charge transfer and atomic charges: The results we obtained for guest–frame charge transfer (CT) are at variance with those from previous studies. Bentien et al.[10] combined information from XANES spectra of $A_8Ga_{16}Ge_{30}$ (A = Sr, Ba) with the analysis of the X-ray electron densities of these clathrates using the MEM method. Spherical integration around the guest atom positions of the difference between the nonuniform prior density and the MEM density supported neutral Sr atoms in the larger cages of $Sr_8Ga_{16}Ge_{30}$, although this same method, when applied to the MEM density of NaF, greatly underestimated (ca. 0.2 e) the complete valence charge transfer that is thought to occur in such an ionic crystal. Reliable MEM charge estimates for the smaller cages of the Sr clathrate and for both cages of the Ba clathrate could not be obtained due to experimental and modelling problems.[45] Instead, the XANES spectra of $A_8Ga_{16}Ge_{30}$ at the K-edge of Sr and at the L_{III}-edge of Ba supported[10] an Sr atom close to neutrality and a Ba atom much more positively charged, when compared with the corresponding spectra for Sr metal and $Sr(OH)_2\cdot 8H_2O$ and Ba metal and BaO.

Blake et al.[9] showed for a number of clathrates, including those of the present study, that the formation of $A_8B_{16}C_{30}$ from A_8 and $B_{16}C_{30}$ takes place through the donation of 16 electrons per unit cell from the valence bands of A_8 into the empty bands of $B_{16}C_{30}$. However, since the spatial charge distribution of the eight donor orbitals of A_8 was found to be very similar to that of the eight acceptor orbitals of $B_{16}C_{30}$, the authors concluded[9] that the guest atoms are *charge donors* but *not ionic* in these clathrates. Their argument is based on the distinction they made between *charge donation*—the flow of electrons from one set of orbitals to another set—and *charge transfer*, defined as the physical displacement of electrons from one region of three-dimensional (3D) space to another. Thus, in the terminology of Blake et al. charge donation and charge transfer will obviously coincide whenever the donor and the acceptor orbitals are located in different spatial regions.

While the above distinction yielded a useful and simple model for the mechanism of guest–framework interaction in the $A_8B_{16}C_{30}$ clathrates, it cannot provide, in general, a correct assignment for the electronic charge transferred from one set to another set of atoms in a given system.[15] Charge partitioning (and as a consequence charge transfer) is not a matter of position, but instead of the physical properties that are associated with such a position. Indeed, properties at a point $\boldsymbol{r}$ in 3D space which is not devoid of particles are a direct consequence of the space(time)-averaged distribution of the particles present in the space, rather than an intrinsic characteristic of the geometrical location of $\boldsymbol{r}$. If the number and/or type of particles constituting a system is changing, the properties at a given point vary, and the electron density at this point may no longer be apportioned to the same atom as before if one uses the QTAIM recipe. It is thus clear that the atomic boundaries within the 3D spaces of the A_8 and $B_{16}C_{30}$ sublattices and the clathrate lattice will differ among each other, even if the atomic species common to these systems are placed in the same geometrical locations with respect to a common reference frame.[46] This argument against definition of charge transfer based only on geometrical considerations can be cast in a rigorous way within QTAIM. This theory can be formulated[16, 47] in terms of the field-theoretical derivation of the principle of stationary action due to Schwinger.[48] One of the important consequences of the application of such a principle to an open system is that both the atomic and local forms of each theorem[49] obtained from the Heisenberg equation of motion for any observable are expressed in terms of a "dressed" density.[15–16] This is a density distribution in real space for a given property, say force or energy, that results

from replacing the property for a single particle at some point in space with a corresponding density that describes the average interaction of a particle with all the remaining particles in the system. In a stationary state, a dressed density m associated with an operator $\hat{M}$ is given by Equation (1),

$$m(\boldsymbol{r}) = \int d\tau' \psi^* \hat{M} \psi \quad (1)$$

where $\int d\tau'$ denotes the averaging of $\hat{M}$ over the coordinates of the remaining particles and the sum over all spins. When $\hat{M} = 1$, one obtains the definition of the electron density. The boundary surface S of a proper open system Ω, a subsystem obeying quantum mechanics, is defined[15] in terms of the topological properties of the electron density as in the equation $(\nabla\rho(\boldsymbol{r}_s) \cdot \boldsymbol{n}(\boldsymbol{r}_s) = 0, \forall \boldsymbol{r}_s \in S)$. For $\hat{M} = -\nabla\hat{V}$, one obtains the Ehrenfest force $\boldsymbol{F}(\boldsymbol{r})$,[50] which is the classical electrostatic force exerted on the electron density at $\boldsymbol{r}$ by the nuclei and by the average distribution of the remaining electrons in the total system (the operator $-\nabla\hat{V}$ represents the gradient taken with respect to the coordinates of the electron located at point $\boldsymbol{r}$ of the total potential energy operator $\hat{V}$ that describes all of the interactions within a system). The Ehrenfest force enters the atomic force theorem[49] and its virial $V(\boldsymbol{r})$,[15, 51] the potential energy density of an electron at $\boldsymbol{r}$, provides the shortest range description for the interactions experienced by an element of the density.[52]

As pointed out earlier and exemplified here, both the definition and the description of the physics of a proper open system are carried out in terms of dressed densities, that is, quantities which are functions of the average space(time) distribution of all the particles in the total system. It is thus clear that the evaluation of the charge of an atom implies a definition of its electronic charge catchment basin, whose shape and properties depend on dressed densities and not on geometrical considerations. When only the latter are used, as in the MEM study by Bentien et al.[10] and in the theoretical study by Blake et al.,[9] one obtains estimates of the guest–host charge transfer that may totally differ from those derived by using a partitioning based on quantum mechanics, as performed in the present study.

It is worth noting that the debate on the definition of charge transfer has a long history,[53] which dates back to the early days of X-ray crystallography, when experimentalists such as W. L. Bragg, R. W. James, P. Debye, and P. Scherrer were already using the concept of electron distribution in their papers,[54, 55] largely anticipating the quantum mechanical probabilistic interpretation given by Born in 1926. X-ray crystallographers were interested in the origin of the bond in ionic crystals such as NaCl. The fact that "Bragg spectra" (diffraction data) of KCl showed the absence of "even" reflections seemed to imply that K and Cl have the same number of electrons or, in other words, that atoms are present as monovalent ions. However, the accuracy of measurements was not deemed sufficient for such a conclusion; moreover, in the crystal of NaF, consisting of much lighter atoms, the mixed reflections were not absent, owing to the different thermal motion of the two ions.[54] The real problem, however, was not only the treatment of the effect of the thermal motion and especially of extinction effects, which prevented the extrapolation to zero scattering angle of the atomic form factors of the two kinds of atoms.[55] Indeed, Bragg et al., in a study on the distribution of electrons around the nucleus in the sodium and chlorine atoms, wrote[55] "Can we tell from the atomic form factors whether their maxima are at 10 (for Na) and 18 (for Cl) or at 11 and 17 respectively? (…) If all the electrons were grouped close to the atomic centers, and if the transference of an electron meant that one electron passed from the Na group to the Cl group, then a solution (…) might be possible. The electron distribution we find extends, on the other hand, right through the volume of the crystal. The distance between Na and Cl centers is 2.81 Å and we find electron distributions 1 Å from the center in sodium and 1.8 Å from the center in chlorine. If the valency electron is transferred from the outer region of one atom to that of the other, it will still be in the region between the two atoms for the greater part of the time". To summarize: in the early days of the electron-distribution era, it was already becoming clear that charge transfer can not be defined from geometrical considerations only. Other criteria, not yet known at that time, had to be brought to the fore.[16]

Charge donation and charge rearrangement: We have thus far discussed how different CT definitions may lead to different estimates of the guest atom ionicity in clathrates and how our physical approach does not support neutral guest atoms. In the following we analyse 1) whether our results confirm or disprove the other conclusion by Blake et al.,[9] that the A atoms act as charge donors (see above for definition), and 2) the extent of charge rearrangement, that is, the point-to-point electron density change, on passing from the IAM to the ab-initio density in $A_8Ga_{16}Ge_{30}$ (A = Sr, Ba).

The density of states (DOS) of $A_8Ga_{16}Ge_{30}$ (A = Sr, Ba) at B1 geometries and near the Fermi level is shown in Figure 3. Both the total DOS and projections on the different sets of contributing atoms (Ge, Ga, A) are reported (Figure 3). Sr and Ba both provide negligible contributions to the occupancy of the valence states close to the Fermi level, while their contribution to the conduction states close to such an energy level is dominant. This result agrees with the finding by Blake et al.[9] that the guest A atoms are charge donors. It also confirms that our wave function, obtained within a different ab initio model, is able to reproduce the relevant features of the total DOS and band structure of this previous study.[9] Thanks to the use of a local basis set, however, we are able to single out the contributions to the total DOS from the different set of atoms with no need to resort to the study of the band (or DOS) structures of the sublattices composing the clathrate and to use a frozen approximation when combining the bands from the various sublattices. Atomic projections of the DOS are evaluated within CRYSTAL code by using a Mulliken-type approach. This approach, contrary to the QTAIM approach based on a real space partitioning, defines atomic projections of a system property such as the total number of electrons in terms of a partitioning of contributions of given subsets of the basis set. Since for the systems investigated in the present work, QTAIM atomic charges are very similar to those obtained with Mulliken's criterion, we

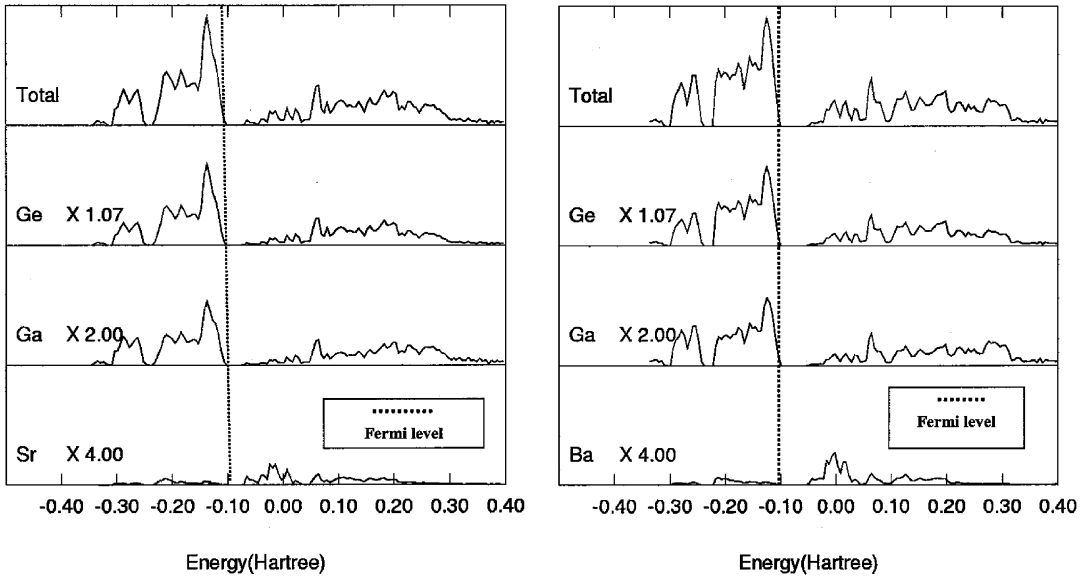

Figure 3. Density of states (DOS) of $A_8Ga_{16}Ge_{30}$ (left: A = Sr; right: A = Ba) at B1 geometries and near the Fermi level. Total DOS and their projections on the different sets of contributing atoms (Ge, Ga, A) are reported in arbitrary units. The scale factor for each projection was chosen so as to compare on the same scale the average single-atom contribution to the DOS from each set.

are confident that the reported atomic DOS projections are not significantly dependent on the basis set. On these grounds, we can thus safely conclude that the guest atoms are both charge donors and ionic in the clathrates studied here.

Figures 4 and 5 detail the spatial charge rearrangement that takes place on passing from the IAM to the ab initio model in planes containing a guest A atom and neighbouring framework atoms or A atoms belonging to different cages. We report the plots only for A = Sr, since those for A = Ba are qualitatively similar. Figure 4 displays the contour plots for the density (top) and for the Laplacian (middle) for the ab initio (left) and IAM (right) models. Plots refer to a plane containing an Sr atom in a 20-atom cage and two Ge atoms at *i* and *k* sites (PC symmetry labeling), one of which is linked to Sr by a bond path (Ge(*i*), 3.46 Å from Sr). Also reported in the same figure is the (ab initio minus IAM) electron density (bottom, left) and Laplacian density (bottom, right) in the same plane. While it is clear that the largest changes brought about by the atomic interactions are located along the covalent bonds of the framework, appreciable charge rearrangements also occur within the interior of the cage. The electron distribution around the Sr atom in the IAM model is more expanded and less spherical, as a result of the overlap of the valence frozen density, than the "real" density. The region around Sr in the density-difference map is entirely charge-depleted, with the most negative contour being equal to -0.08 a.u. (for the sake of clarity, the contour levels increase in thickness with increasing absolute value in the electron-density difference map).[56] From these data, it is clear that the calculated charge for Sr (Table 4) is the result of both charge depletion in the Sr basin and of a decrease in volume of the Sr catchment region compared to that of the IAM density (the BCP is closer to the Sr nucleus by about 0.2 Å in either kind of cage). The former contribution is the "spatial" charge transfer discussed by Blake et al.,[9] although calculated with respect to another reference system (IAM in our case, the Sr_8 sublattice in ref. [9]). The electron depletion within the Sr basin makes a significant contribution to the positive charge calculated for the guest atom. Indeed, if one assumes a spherical Sr basin with radius equal to the average BCP distance from the Sr nucleus (1.67 Å) and an average density difference of 0.04 a.u. within the basin, one would obtain an electron depletion equal to $0.8\,e^-$, which is about half of the charge transferred from Sr to the framework (Table 4). Figure 5 displays similar functions to Figure 4 but for a plane containing an Sr atom in the 20-atom cage and two other Sr atoms in the 24-atom cages. The electron and Laplacian density of the two kinds of Sr atoms are very similar, as is their (ab initio minus IAM) electron density difference (bottom, left). Contrary to Figure 4, the bottom right panel shows the ab initio electron-density difference between $Sr_8Ga_{16}Ge_{30}$ and the Sr_8 sublattice. Taking the Sr_8 sublattice as a reference system, one finds that in the clathrate the electron charge is depleted around the Sr atom within a distance of about 1.8 Å from the nucleus (i.e., about 0.15 Å farther than the BCPs), while it is accumulated at larger distances. Even with respect to this reference system, the electron depletion within the Sr basins appears to be noteworthy.

Chemical bonding: The electron-density description of the frame–guest interactions presented above can be discussed in view of previous considerations by Blake et al.[9] These authors found a significant binding energy (>4 eV per guest) for the frame–guest interaction, although both the calculated low frequencies ($40-100\,cm^{-1}$) for the motion of the guest atom in the cages and the lack of any structural evidence for "directed" bonding suggested weak bonding and a low host–guest binding energy. Blake et al. concluded that the "large binding energy obtained in their calculations indicate that the guest–frame bond is unusual", since "the guest forms a strong

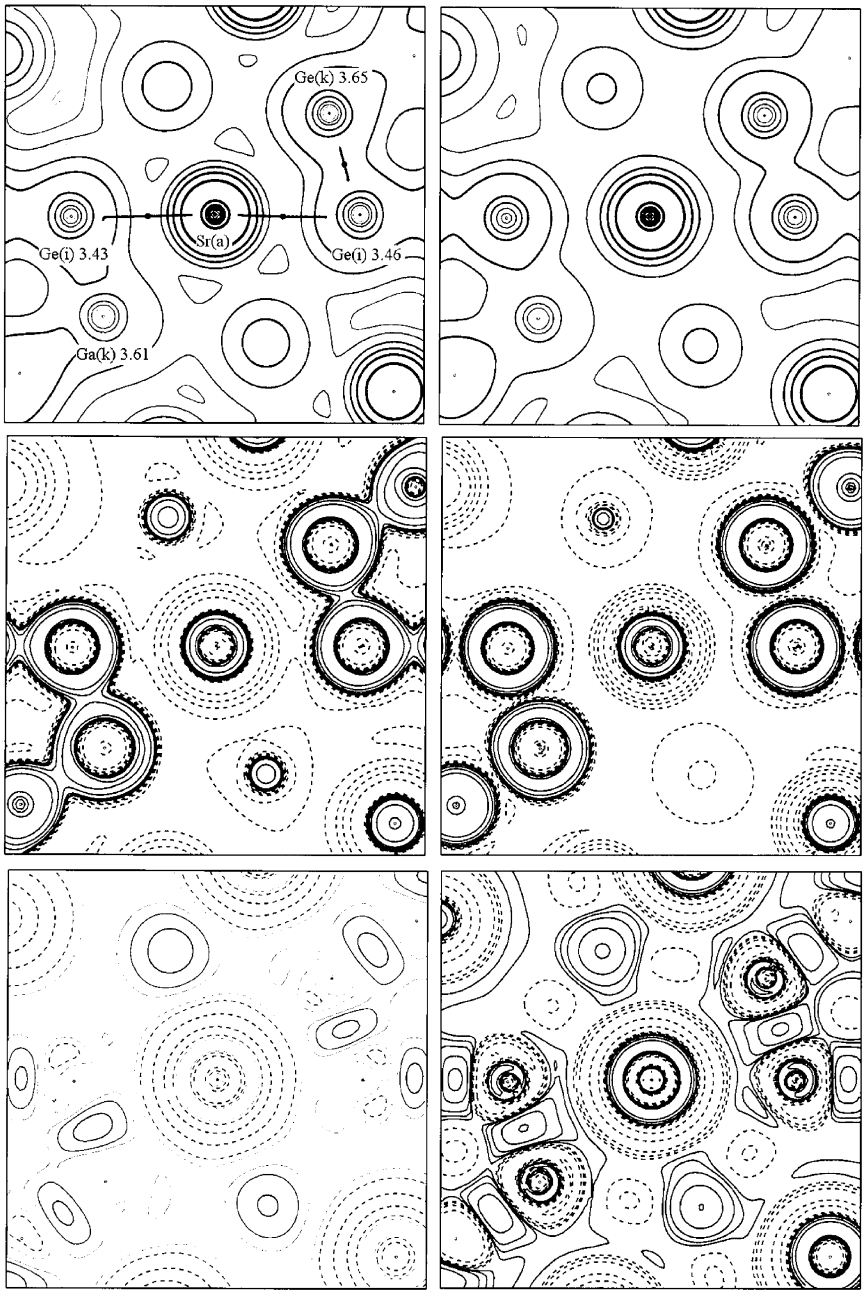

Figure 4. Contour maps of the electron density ρ (top) and of the negative Laplacian ($L = -\nabla^2\rho$, middle) for the ab initio (left) and the IAM model (right) of $Sr_8Ga_{16}Ge_{30}$ in the B1 geometry. The functions are plotted in a plane containing an Sr atom at position *a* (20-atom cage) and two Ge atoms at positions *i* and *k* at distances of 3.46 and 3.65 Å from the Sr atom. Positions are labeled as in the parent clathrate (see text). The nuclei of the Ge and Ga atoms at the left of the central Sr atom are less than 0.1 Å from the plotted plane. The overlaid bond paths (top, left) denote the Ge atoms bonded to the Sr atom. The Ge and Ga atoms at *k* positions, which are at distances from Sr greater than 3.6 Å, are not bonded to the central Sr atom. The bottom panels report the (ab initio minus IAM) electron density (left) and Laplacian density (right) in the same plane. Contour levels at ± 2, ± 4 and $\pm 8 \times 10^n$ a.u. ($n = 0$ to -3). Dashed contours denote negative contour values. In the case of the ρ difference density (bottom, left) the contour levels increase in thickness with increasing absolute value. The most negative and positive contour around Sr are -0.08 a.u. and 0.04 a.u., respectively. In the difference densities the negative contours are associated with regions in which the ab initio model has a lower value of ρ (bottom, left) or of L (bottom, right) compared with the IAM model. The positive contours around Sr are at least 2.3 Å from the Sr nucleus (cf. the average distance of a BCP from the nucleus of about 1.66 Å).

bond with the whole cage rather than having a customary pair wise bonding between the guest and a specific frame atom. This happens partly because the valence orbitals of the guest atom overlap strongly with those of all the frame atoms". According to our analysis, the significant host–guest binding energy is mainly due to CT from the guest to the host. Thus, although we confirm that the "guest–frame bond is a bond with the whole cage",[9] we disagree on the premises which led to such a conclusion. This bond should be mostly electrostatic in nature because the guest atom is far from neutral. Electron-density topological properties at the A–Ga(Ge) BCPs confirm this picture. Even if the occurrence of these BCPs and their density values indicate that the guest–host interaction is somewhat "directional" (and especially so in the 24-atom cages), the locations and properties at these BCPs are typical of a closed-shell ionic interaction. If one assumes similar electron–electron integrals for the valence electrons of Ba_8-$Ga_{16}Ge_{30}$ and for a system comprising Ba_8 and $Ga_{16}Ge_{30}$, it can be shown that the large Ba binding energy seen in Ba_8-$Ga_{16}Ge_{30}$ is consistent with difference in the respective electron affinities of the Ba_8 and $Ga_{16}Ge_{30}$ sublattices. A crude estimate along these lines leads to a binding energy of 3.5 eV.[57] This confirms the picture that the stability of the clathrate is attributable to the electron-donating role played by the encapsulated metal atom.

It is also interesting to relate the observed strengthening (Table 7) of the Sr–host interactions in the larger cages with the calculated[9] frequency of the cage "rattling" motion in the clathrates. Frequencies for Sr in the larger cages were calculated[9] to be larger than for the smaller cages, consistent with the stronger Sr–frame interactions found by us in the larger cages. The opposite was true for Ba, also in agreement with the BCP data reported in Table 7. The strong asymmetry of the potential energy curve calculated for the displacement of Sr in the 24-atom cages is

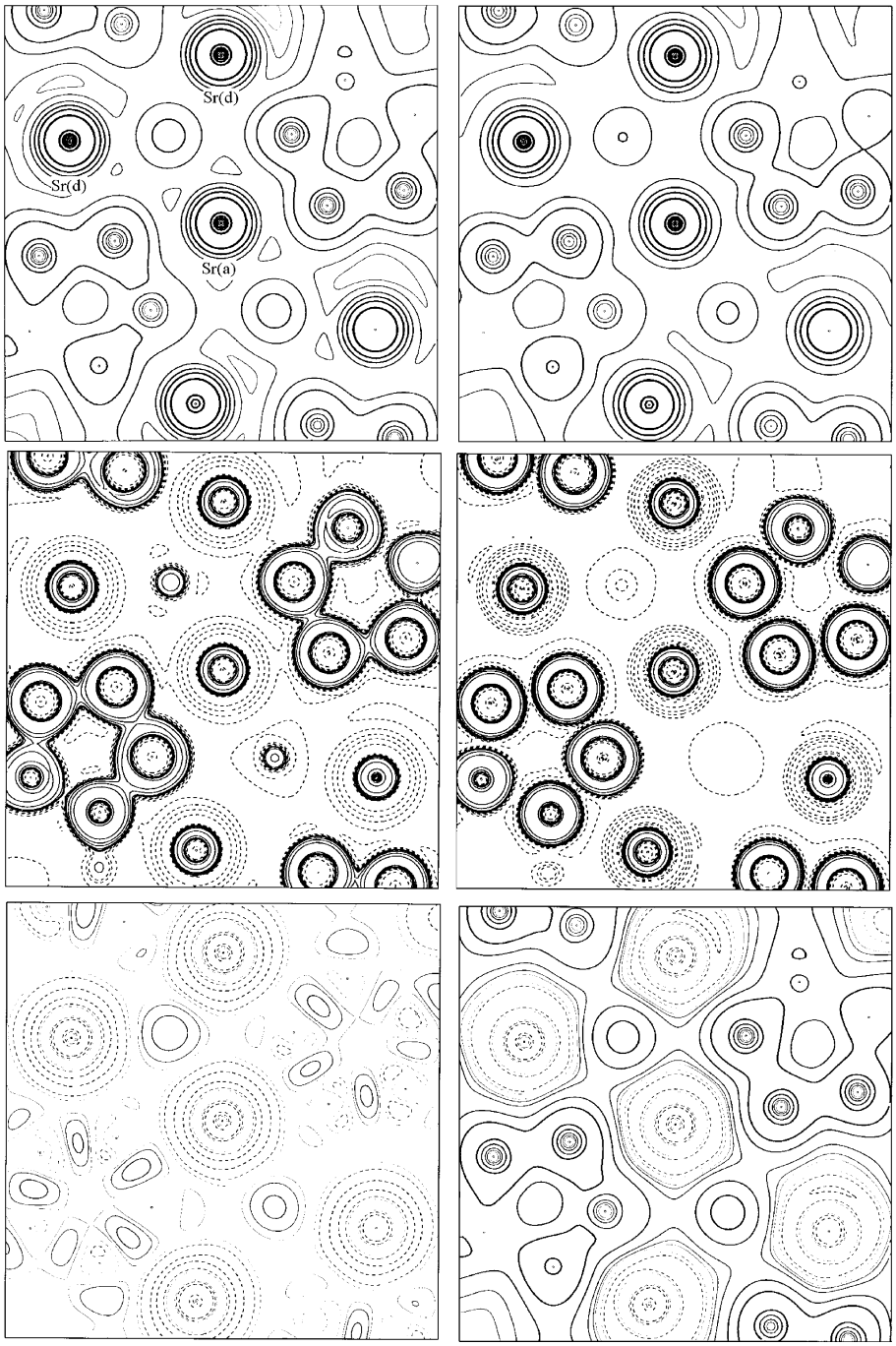

Figure 5. Contour maps of the electron density ρ (top) and of the negative Laplacian ($L = -\nabla^2\rho$, middle) for the ab initio (left) and the IAM model (right) of $Sr_8Ga_{16}Ge_{30}$, in the B1 geometry. The functions are plotted in a plane containing three Sr atoms, one at position *a* (20-atom cage) and two at positions *d* (24-atom cage). Positions are labeled as in the parent clathrate (see text). The bottom panels report the (ab initio minus IAM) electron density (left) and the ($Sr_8Ga_{16}Ge_{30}$ minus Sr_8) ab initio electron density difference (right). Both these difference densities were calculated for the B1 geometry of the clathrate. Contour levels as in Figure 4. In the case of the ρ difference density the contour levels increase in thickness with increasing absolute value. The most negative contour around Sr in the (ab initio minus IAM) electron density (bottom, left) is -0.08 a.u., while the most negative and positive contours around Sr in the ($Sr_8Ga_{16}Ge_{30}$ minus Sr_8) ab initio electron density difference (bottom, right) are -0.08 and 0.04 a.u., respectively.

nicely mirrored in the asymmetry of the guest–host bonding interactions found in these cages. It is the possibility to increase the strength (and covalent character) of these interactions which is ultimately responsible for the disordered Sr site, revealed experimentally by the MEM deformation density of the 24-atom cages.[10]

Effect of pressure: In view of the increase in the thermoelectric figure of merit *ZT* of *n*-doped $Sr_8Ga_{16}Ge_{30}$ induced by external pressure,[13] we looked at whether charge transfer might be affected by pressure and whether charge transfer is related to the Seebeck coefficient *S*. According to Meng et al., the threefold *ZT* enhancement at 7.5 GPa should mostly be ascribed to the observed increase, by a factor of 1.85, in the magnitude of the Seebeck coefficient at this pressure.[58] In our preliminary investigation, a crude structural model was assumed, with the reduction of cell parameters being the only geometrical change due to compression at 4.3 and 7.5 GPa.[59] This choice of geometry was deemed reasonable, since diffraction measurements[13] on a hydrostatically compressed sample showed that up to 7.5 GPa the crystal structure remains the same as at ambient pressure, and hence the increase in *S* is not associated with a crystallographic phase transition. Evaluation of atomic basins and net charges indicate a very small decrease, by about 0.01 e, in the charge transfer from the guest to the framework on compression at the highest pressure of 7.5 GPa. The total DOS for the compressed clathrate and the contribution from Sr atoms is hardly changed with respect to that reported in Figure 3 for the unperturbed clathrate. On the other hand, the electron density at the Sr–Ge(Ga) BCPs rises by about 7–10%, in agreement with an enhanced Sr–framework interaction in the compressed clathrate.

We conclude that the Sr guest is almost completely ionized and continues to act as a charge donor under an applied external pressure. For this crude geometrical model and the

range of investigated pressures, there is no direct relationship between charge transfer and the increase in the thermopower *S*. These results seem to rule out the possibility of simulating the effect of external pressure by suitable chemical tuning to increase or decrease the CT from the host metal to the framework. Note, however, that the sample investigated by Meng et al. had a large stoichiometry deviation ($Sr_{6.38}Ga_{15.64}Ge_{30}$), with incomplete occupation of cages by the Sr guest. This structural defect could significantly affect both the geometrical distortions and the charge transfer on compression. The importance of the lattice composition for *ZT* and other quantities of interest for thermoelectric behaviour was recently reported by Bryan et al.[60] for $Ba_xGa_yGe_z$ clathrates of different compositions and chemical purity.

Conclusion

Our theoretical study indicates that in the type I inorganic clathrates $A_8Ga_{16}Ge_{30}$ (A = Sr, Ba), the guest atoms are largely ionized in both the smaller 20-atom cages and the larger 24-atom cages. The influence of the kind of Ga sitings on the host–guest CT seems rather limited, in view of the similar CT calculated for the B1 and B3 geometries of the clathrates. The multiwavelength diffraction experiment also supports similar oxidation states for the Sr atoms in the different cages, with an adsorption edge similar to that found in the Sr K-edge XANES spectra[10] of $Sr(OH)_2 \cdot 8H_2O$.

This result contradicts previous experimental and theoretical studies claiming almost charge neutrality of the guest atoms. We show that such discrepancy is related to the definitions used for electron transfer. Use of a definition based on electron displacement in space,[9–10] something that may be better termed "charge rearrangement", does not account for the local change in the virial of forces acting on an element of the charge density and, consequently, for the variations in the shape and volume of the atomic catchment regions due to the change in the number and average locations of particles in the system. In our case, we show that charge rearrangement underestimates charge transfer when this is evaluated within the rigorous quantum mechanics framework provided by QTAIM.

Using information from the total density of states and from its atomic projections, we confirmed the previous conclusion[9] that the guest atoms act as charge donors in these clathrates, electrons being taken from the highest valence bands of the A_8 sublattice and placed into orbitals of the $Ga_{16}Ge_{30}$ sublattice. Due to the use of a local basis set, we come to this conclusion without resorting to band analysis of the sublattices composing the clathrate and the use of the frozen-band approximation. The ionic character of the guest atoms demonstrated here, along with confirmation of their charge-donor behaviour, fully reconciles the theoretical analysis with the structural chemist's view of these type I clathrates as Zintl phases.

A detailed description of the guest–host interactions has been formulated in terms of the electron density topology. The larger cages exhibit a smaller number of interactions than the 20-atom cages. The notable displacement of the guest atoms in the larger cages appears to be driven by the energy gain due to the formation of guest–host interactions of similar (Ba) or much greater (Sr) strength than in the smaller cages. The guest–host interactions have a closed-shell nature. The large binding energy found for the frame–guest interaction (ca. 4 eV per guest),[9] is consistent with electron affinity of the $Ga_{16}Ge_{30}$ sublattice relative to the average energy of the valence electrons in Ba_8.

Preliminary investigations on a perfectly stoichiometric clathrate appear to exclude any important relationship between the application of external pressure and the host–guest charge transfer (or the extent of "charge donation" from the guest). This result seems to rule out the possibility of simulating the effect of external pressure by suitable chemical tuning to increase or decrease the CT from the host metal to the framework. However, strong deviation from stoichiometry, as present in the sample investigated by Meng et al.,[13] could possibly change this picture.[60]

Acknowledgement

This work was supported by the European Community under contract number G5RD-CT2000-00292, NanoThermel project. Special thanks go to all partners in this project: M. Muhammed, M. Toprak, Y. Zhang and K. Billquist (Royal Institute of Technology, Stockolm, Sweden), M. Rowe and S. Williams (NEDO Laboratory for Thermoelectric Engineering, Cardiff, U.K.), C. Stiewe, D. Platzek and E. Müller (German Aerospace Center, Cologne, Germany), M. Christiansen (University of Aarhus, Denmark), A. Palmqvist (Chalmers University of Technology, Goteborg, Sweden), G. Noriega (CIDETE, Spain) and L. Holmgren (LEGELAB, Sweden). Dan Bryan, Silvia Capelli and Philip Pattison are gratefully acknowledged for significant help with the multiwavelength diffraction experiment, and the ESRF is thanked for beam time at the Swiss-Norwegian beamline. One of us (C.G.) thanks Dirk Feil for pointing out the analogies between the present debate on charge transfer in clathrates and that, in the early days of X-ray crystallography, on charge transfer in diatomic ionic crystals.

[1] G. A. Slack in *CRC Handbook of Thermoelectrics*, (Ed.: D. M. Rowe), CRC, Boca Raton, **1995**, pp. 407–440.
[2] G. A. Slack, *Mater. Res. Soc. Symp. Proc.* **1997**, *478*, 47.
[3] J. J. Dong, O. F. Sankey, G. K. Ramachandran, P. F. McMillan, *J. Appl. Phys.* **2000**, *87*, 7726–7734.
[4] J. J. Dong, O. F. Sankey, and C. W. Myles, *Phys. Rev. Lett.* **2001**, *86*, 2361–2364.
[5] G. S. Nolas, C. A. Kendziora, *Phys. Rev. B* **2000**, *62*, 7157–7161.
[6] J. L. Cohn, G. S. Nolas, V. Fessatidis, T. H. Metcalf, G. A. Slack, *Phys. Rev. Lett.* **1999**, **82**, 779–782.
[7] B. B. Iversen, A. E. C. Palmqvist, D. E. Cox, G. S. Nolas, G. D. Stucky, N. P. Blake, H. Metiu, *J. Solid State Chem.* **2000**, *149*, 455–458.
[8] N. P. Blake, L. Møllnitz, G. Kresse and H. Metiu, *J. Chem. Phys.* **1999**, *111*, 3133–3144.
[9] N. P. Blake, D. Bryan, S. Latturner, L. Møllnitz, G. D. Stucky, H. Metiu, *J. Chem. Phys.* **2001**, *114*, 10063–10074.
[10] A. Bentien, A. E. C. Palmqvist, J. D. Bryan, S. Latturner, G. D. Stucky, L. Furenlid, B. B. Iversen, *Angew. Chem.* **2000**, *112*, 3759–3762; *Angew. Chem. Int. Ed.* **2000**, *39*, 3613–3616.
[11] N. P. Blake, S. Latturner, D. Bryan , G. D. Stucky, H. Metiu, *J. Chem. Phys.* **2001**, *115*, 8060–8073.
[12] G. S. Nolas, T. J. R. Weakley, J. L. Cohn, R. Sharma, *Phys. Rev. B* **2000**, *61*, 3845–3850.
[13] J. F. Meng, N. V. Chandra Shekar, J. V. Badding, G. S. Nolas, *J. Appl. Phys.* **2001**, *83*, 1730–1733.
[14] E. Zintl, G. Brauer, *Z. Phys. Chem. Abt. A* **1933**, *20*, 241.

[15] R. F. W. Bader, *Atoms in Molecules: A Quantum Theory*, Oxford University Press, Oxford, **1990**.
[16] R. F. W. Bader *Phys. Rev. B* **1994**, *49*, 13348.
[17] B. B. Iversen, personal communication.
[18] W. B. Pearson, *Handbook of Lattice Spacing and Structures of Metals and Alloys*, Pergamon Press, London **1967**.
[19] R. W. G. Wyckoff, *Crystal Structure*, Wiley, New York, **1963**.
[20] V. R. Saunders, R. Dovesi, C. Roetti, M. Causà, N. M. Harrison, R. Orlando, C. M. Zicovich-Wilson, CRYSTAL98, User's Manual, University of Torino, Torino, **1998**.
[21] J. P. Perdew, Y. Wang, *Phys. Rev. B* **1992**, *45*, 13244.
[22] A. D. Becke, *Phys. Rev. A*. **1988**, *38*, 3098.
[23] W. R. Wadt, P. J. Hay, *J. Chem. Phys.* **1985**, *82*, 284–298.
[24] S. F. Vyboishchikov, A. Sierralta, G. Frenking, *J. Comput. Chem.* **1996**, *18*, 416–429.
[25] P. J. Hay, W. R. Wadt, *J. Chem. Phys.* **1985**, *82*, 299–310.
[26] W. J. Hehre, L. Radom, P. von R. Schleyer, J. A. Pople, *Ab Initio Molecular Orbital Theory*, Wiley-Interscience, New York, **1986**, and references therein.
[27] M. P. Habas, R. Dovesi, A. Lichanot, *J. Phys. Condens. Matter* **1998**, *10*, 6897–6909.
[28] a) J. S. Binkley, J. A. Pople, W. J. Hehre, *J. Am. Chem. Soc.* **1980**, *102*, 939; b) K. D. Dobbs, W. J. Hehre, *J. Comput. Chem.* **1986**, *8*, 861.
[29] C. M. Zicovich-Wilson, LoptCG (Shell procedure for numerical gradient optimizations), Instituto di Tecnologia Quimica, UPC-CSIC, Spain, **1998**.
[30] C. Gatti, TOPOND98 User's Manual, CNR-ISTM, Milano, **1999**.
[31] P. Coppens, *Synchrotron Radiation Crystallography*, Academic Press, London, **1992**.
[32] J. L. Hodeau, V. Favre-Nicolin, S. Bos, H. Renevier, E. Lorenzo, J. F. Berar, *Chem. Rev.* **2001**, *101*, 1843–1868.
[33] The quality of the crystal was excellent, with typical ω scan peak widths of 0.01° (FWHM). The crystal was obtained by crushing larger single crystals synthesized with the flux method.[10]
[34] For the (3, 5, 6), (4, 8, 12) and (6, 9, 9) reflections all symmetry-equivalent reflections were collected (48, 48 and 24 respectively) to enable an accurate empirical absorption correction.
[35] Since the anomalous scattering contribution is almost constant as a function of scattering angle, the high-order data will have a relatively larger intensity change across the absorption edge due to anomalous scattering effects.
[36] The positional and thermal parameters obtained from the short-wavelength data set were in excellent agreement with values obtained from extensive conventional single-crystal X-ray diffraction data.[33]
[37] The scale factor and the extinction parameter have about 60% correlation with each other, but only little correlation with the f' parameters. The refined f' values are quite insensitive to changes in the reference structural model. If the Sr(2) single-site structural model refined by Nolas et al.[12] is used in refinements of f', the numerical values of f' change slightly, but the overall shapes of the curves are preserved. However, use of the structural model of Nolas et al. degrades the fits by 1–2% on R_{F^2}. The f' values do not change if the low-order reflections most affected by extinction are removed from the data set, or if the Sr occupancies are arbitrarily reduced to 98%.
[38] $Z_{eff} = 10$ for Sr and Ba in our PP and AEPP calculations.
[39] We verified whether or not our results are seriously affected by the basis set modifications we made to speed up computations. Indeed, for the Sr-PC, the net positive charge of the Sr atoms decreases (by ca. 0.09 e) rather than increasing on removal of the outermost Gaussian function of the original Hay–Wadt Sr basis set.
[40] Using the subsystem hypervirial theorem and the commutator of H and r^2, the Hamiltonian operator and the square of the radial distance of the electron in the free atom from the nuleus, respectively, one obtains the identity $3N(\Omega) + \int_\Omega (\boldsymbol{r}\cdot\nabla\rho)\mathrm{d}\tau = \varsigma\rho(\boldsymbol{r})\boldsymbol{r}\cdot\boldsymbol{n}(\boldsymbol{r})$.[15] In a free atom, in which the nucleus acts as the only attractor in the gradient field, the vector $\nabla\rho$ and the radial vector $\boldsymbol{r}$ are parallel and oppositely directed and the integral on the left-hand side reaches its maximum negative value, equal to $-3N(\Omega)$, since for the isolated atom the surface integral vanishes. In a bound atom, formation of chemical bonds distorts $\nabla\rho$ and leads to a smaller overlap of $\boldsymbol{r}$ and $\nabla\rho$ compared to the free atom. The greater the distortion of the gradient vector field, the smaller the overlap of $\boldsymbol{r}$ and $\nabla\rho$ and the larger the difference between the magnitude of the two terms on the left-hand side, which is measured by the integral over the atomic surface. The ratio $\mathrm{SPHD} = \int_\Omega (\boldsymbol{r}\cdot\nabla\rho)\mathrm{d}\tau/[-3N(\Omega)]$ is introduced here as a convenient quantity that attains the value of one for a free atom and in the limit of an extremely loosely bound atom.
[41] a) D. T. Cromer, D. J. Liberman, *J. Chem. Phys.* **1970**, *53*, 1891; b) B. L. Henke, P. Lee, T. J. Tanaka, R. L. Shimabukuru, K. B. Fujikawa, *At. Data Nucl. Data Tables* **1982**, *27*, 1; c) C. T. Chantler, *Radiat. Phys. Chem.* **1993**, *41*, 759.
[42] M. Benfatto, R. Felici, *Phys. Rev. B* **2001**, *64*, 115410.
[43] For the sake of comparison with the bonding features in the B1-geometry clathrates, the cell parameter of the parent clathrates (A = Sr, Ba) in these calculations was set equal to that of the B1 structures.
[44] For the sake of simplicity, here we refer to the (3, –1) CPs as BCPs also in the case of the IAM densities. However, one must bear in mind that the properties at these (3, –1) CPs are not indicative of any bonding, since by definition no bonding takes place in the IAM densities. Moreover, QTAM may not apply to such densities, since they are not derived from a wave function.
[45] MEM charge estimates for Sr in the 20-atom cage and for Ba in either kind of cage were strongly affected by the few low-order reflections which suffer from extinction, as well as by the exact site occupancy.
[46] There can be regions of the 3D space in which the physical properties of one of the component sublattices at limit become equal to those in the clathrate, but this obviously can not be true in general.
[47] R. F. W. Bader, *Can. J. Chem.* **1998**, *76*, 973–988.
[48] J. Schwinger, *J. Phys. Rev.* **1951**, *82*, 914.
[49] R. F. W. Bader, P. L. A. Popelier, *Int. J. Quant. Chem.* **1993**, *45*, 189–207.
[50] P. Z. Ehrenfest, *Physik* **1927**, *45*, 455.
[51] R. F. W. Bader, *J. Phys. Chem.* **1998**, *A102*, 7314–7323.
[52] R. F. W. Bader, *Int. J. Quantum Chem.* **1995**, *56*, 409.
[53] P. Coppens, D. Feil in *The Application of Charge Density Research to Chemistry and Drug Design* (Eds.: G. A. Jeffrey, J. F. Piniella), NATO ASI Series *B250*, Plenum Press, New York, **1991**, pp. 7–22.
[54] P. Debye, P. Scherrer, *Phys. Z.* **1918**, *19*, 474.
[55] W. L. Bragg, R. W. James, C. H. Bosanquet, *Phil. Mag.* **1922**, *44*, 433–449.
[56] Positive regions in the density difference are as far from the Sr nucleus as 2.3 Å (to be compared, Table 6, with the average BCP distance from the nucleus of about 1.66 Å), with the maximum positive contour equal to 0.04 a.u.
[57] N. P. Blake, personal communication.
[58] Meng et al.[13] hypothesize that the Wiedemann–Franz law should be applicable to the $Sr_8Ga_{16}Ge_{30}$ clathrate and that its lattice thermal conductivity should not increase by more than a factor of two on compression to 7.5 GPa.
[59] Cell parameters were changed so as to comply with V/V_0, the normalized volume, which is equal to 0.975 at 4.3 GPa and 0.946 at 7.5 GPa.[13]
[60] J. D. Bryan, N. P. Blake, H. Metiu, B. B. Iversen, R. D. Poulsen, A. Bentien, *J. Appl. Phys.* **2002**, *92*, 7281–7290.
[61] R. H. Blessing, *J. Appl. Crystallogr.* **1989**, *22*, 396–397.

Received: February 10, 2003 [F4837]